

Solution structure and siRNA-mediated knockdown analysis of the mitochondrial disease-related protein C12orf65

Hiroyuki Kogure,¹ Yusuke Hikawa,¹ Mamoru Hagihara,¹ Naoya Tochio,² Seizo Koshiba,² Yusuke Inoue,¹ Peter Güntert,^{3,4} Takanori Kigawa,^{2,5} Shigeyuki Yokoyama,^{2,6} and Nobukazu Nameki^{1*}

¹Department of Chemistry and Chemical Biology, Graduate School of Engineering, Gunma University, Kiryu, Gunma 376-8515, Japan

²RIKEN Systems and Structural Biology Center, Tsurumi, Yokohama 230-0045, Japan

³Institute of Biophysical Chemistry, Center for Biomolecular Magnetic Resonance, and Frankfurt Institute for Advanced Studies, Goethe University, Frankfurt am Main, Germany

⁴Graduate School of Science, Tokyo Metropolitan University, Hachioji, Tokyo 192-0397, Japan

⁵Department of Computational Intelligence and Systems Science, Interdisciplinary Graduate School of Science and Engineering,

Tokyo Institute of Technology, Yokohama, Kanagawa 226-8502, Japan

⁶Department of Biophysics and Biochemistry, Graduate School of Science, University of Tokyo, Bunkyo-Ku, Tokyo 113-0033, Japan

ABSTRACT

Loss of function of the *c12orf65* gene causes a mitochondrial translation defect, leading to encephalomyopathy. The C12orf65 protein is thought to play a role similar to that of ICT1 in rescuing stalled mitoribosomes during translation. Both proteins belong to a family of Class I peptide release factors (RFs), all characterized by the presence of a GGQ motif. Here, we determined the solution structure of the GGQ-containing domain (GGQ domain) of C12orf65 from mouse by NMR spectroscopy, and examined the effect of siRNA-mediated knockdown of C12orf65 on mitochondria in HeLa cells using flow cytometry. The GGQ domain, comprising residues 60–124 of the 184-residue full-length protein, forms a structure with a 3_{10} - β 1- β 2- β 3- α 1 topology that resembles the GGQ domain structure of RF more closely than that of ICT1. Thus, the GGQ domain structures of this protein family can be divided into two types, depending on the region linking β 2 and β 3; the C12orf65/RF type having a 6-residue π -HB turn and the ICT1 type having an α -helix. Knockdown of C12orf65 resulted in increased ROS production and apoptosis, leading to inhibition of cell proliferation. Substantial changes in mitochondrial membrane potential and mass in the C12orf65-knockdown cells were observed compared with the control cells. These results indicate that the function of C12orf65 is essential for cell vitality and mitochondrial function. Although similar effects were observed in ICT1-downregulated cells, there were significant differences in the range and pattern of the effects between C12orf65- and ICT1-knockdown cells, suggesting different roles of C12orf65 and ICT1 in rescuing stalled mitoribosomes.

Proteins 2012; 80:2629–2642.

© 2012 Wiley Periodicals, Inc.

Key words: flow cytometry; GGQ domain; ICT1; mitochondria; NMR; release factor; ribosome rescue; YaeJ.

INTRODUCTION

Most mitochondrial diseases are caused by defects in enzyme complexes of the oxidative phosphorylation (OXPHOS) system, which comprises five multisubunit enzyme complexes (I–V) encoded by nuclear and mitochondrial genes.¹ The defects are often caused by mutations of nuclear gene products directly or indirectly involved in mitochondrial translation, including mitochondrial elongation factors, mitochondrial ribosomal proteins, and tRNA-modifying enzymes, and these gene

Additional Supporting Information may be found in the online version of this article

Grant sponsor: Grant-in-Aid for Scientific Research (C) from the Ministry of Education, Culture, Sports, Science and Technology (MEXT) of Japan; Grant number: 23570205 (to N.N.); Grant sponsor: Lichtenberg program of the Volkswagen Foundation (to P.G.).

*Correspondence to: Nobukazu Nameki, Department of Chemistry and Chemical Biology, Graduate School of Engineering, Gunma University, 1-5-1 Tenjin-Cho, Kiryu, Gunma 376-8515, Japan. E-mail: nameki@gunma-u.ac.jp

Received 17 April 2012; Revised 27 June 2012; Accepted 5 July 2012

Published online 21 July 2012 in Wiley Online Library (wileyonlinelibrary.com).

DOI: 10.1002/prot.24152

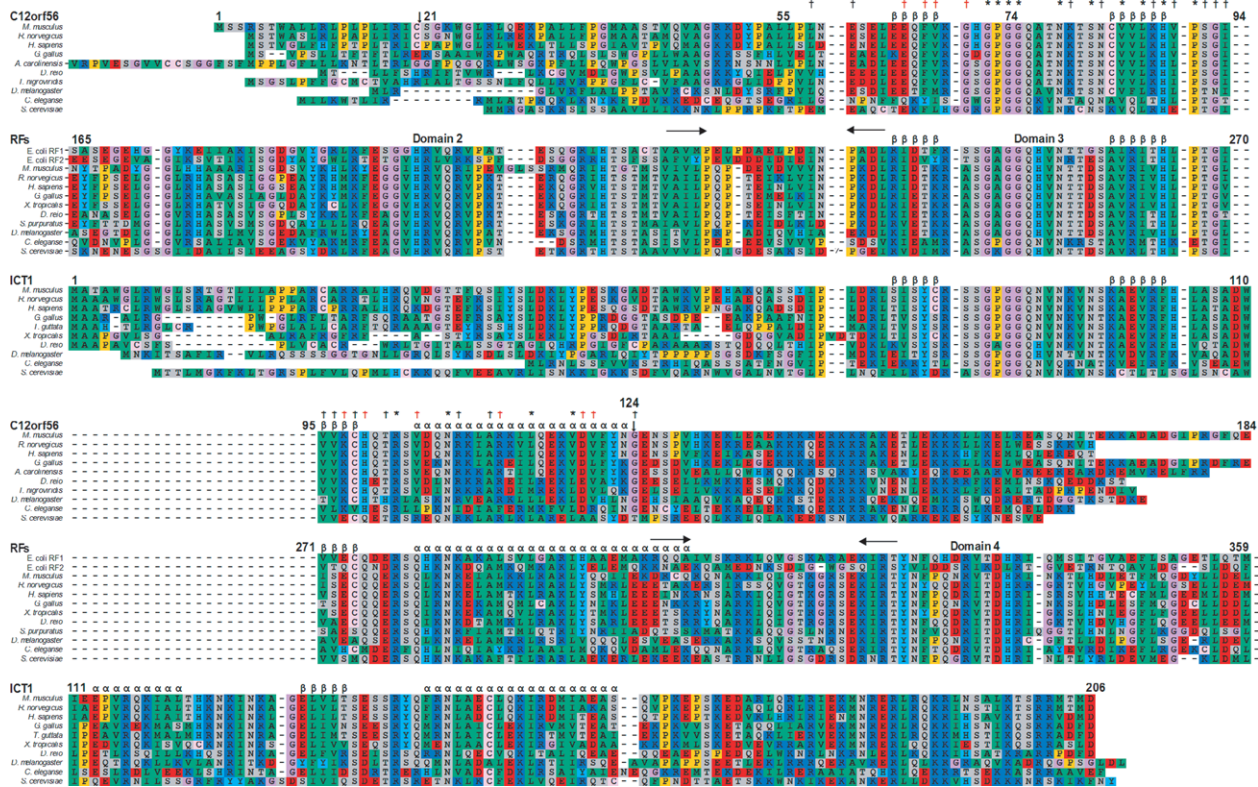


Figure 1

Structure-based sequence alignment of C12orf65 and ICT1 proteins from eukaryotes and of *E. coli* and mitochondrial RFs. Secondary structure elements of the C12orf65 structure determined in this study (PDB ID 2RSM), ICT1 (1J26), and the RF2 structure (1GQE) are indicated. The truncation positions for the mouse C12orf65 protein used in the structure determination are marked by vertical arrows. Asterisks indicate highly conserved residues (>90%) among all of the three proteins from eukaryotes. The code † colored in black indicates highly conserved residues (>90%) among C12orf65 proteins and mtRFs from eukaryotes, and the code † colored in red indicates those among C12orf65 proteins from eukaryotes. Alignments are colored: purple: glycine (G); yellow: proline (P); green: small and hydrophobic amino acids (A, V, L, I, M, F, W); gray: hydroxyl and amine amino acids (S, T, N, Q); red: negatively charged amino acids (D, E); blue: positively charged amino acids (K, R); pink: cysteine (C); cyan: histidine (H) and tyrosine (Y).

defects underlie combined OXPHOS deficiencies.^{2,3} A recent study has revealed that a loss-of-function mutation in a nuclear gene, *c12orf65*, encoding a mitochondrial matrix protein in two unrelated pedigrees caused a decrease in the levels of OXPHOS complexes, leading to encephalomyopathy.⁴ Two different 1-bp deletions in *c12orf65*, both of which result in the same premature stop codon, severely affect mitochondrial translation, resulting in significant decreases of the OXPHOS complexes I, IV, and V, and a smaller decrease of complex III. In contrast, these deletions had no effects on other factors involved in mitochondrial translation such as mRNAs, tRNAs, rRNAs, translation elongation factors, and ribosomal proteins.

According to the Pfam database,⁵ the C12orf65 protein belongs to the RF-1 family as represented by class I peptide release factors (RFs) from bacteria and mitochondria, which are characterized by the presence of a conserved GGQ motif (Gly-Gly-Gln motif) (Fig. 1). The bacterial-type RFs (RF1 and RF2 in bacteria; mtRF1a in

mitochondria) are composed of four domains, each of which has specific roles when bound to a ribosome for translation termination.^{6,7} The GGQ motif is located in domain 3, termed GGQ domain, and the domain interacts with the peptidyltransferase center (PTC) of the large ribosomal subunit to trigger peptidyl-tRNA hydrolysis (PTH), resulting in the release of the nascent polypeptide chain from the P-site-bound peptidyl-tRNA. The catalysis involves the universally conserved GGQ motif residues, which are located in an unstructured loop in a free RF.^{8,9} Crystal structures of the 70S ribosome in complex with RF1 or RF2 demonstrate that the GGQ-containing loop (GGQ loop) of the bound RF adopts a fixed conformation at the PTC, with the GGQ motif residues contributing directly to the PTH activity.^{10,11} RF-1 family proteins are divided into two groups according to the length of the amino acid sequence. One group of proteins with a longer sequence length includes RFs from bacteria and mitochondria (~360 residues), and the other group of proteins with a shorter sequence length

includes C12orf65 and immature colon carcinoma cell transcript 1 (ICT1) (~190 residues), both of which are localized exclusively in mitochondria (Fig. 1).^{4,12,13} C12orf65 and ICT1 lack a structured region that recognizes stop codons like RFs, but in the GGQ domain region, C12orf65 is more similar in sequence to RFs than to ICT1.

Recent studies have revealed roles of ICT1 and the *Escherichia coli* ICT1 homolog YaeJ. ICT1 is an integral component of the mitochondrial ribosome (mitoribosome).¹⁴ Release-factor assays using isolated *E. coli* ribosomes have shown that ICT1 has codon-independent PTH activity via the GGQ motif.¹⁴ Depletion of ICT1 using ICT1-specific siRNA resulted in a reduction of mitochondrial protein synthesis, leading to a loss of cell viability as well as mitochondrial dysfunction.^{14,15} For YaeJ, *in vitro* translation experiments using the *E. coli*-based reconstituted cell-free protein synthesis system have revealed that YaeJ can hydrolyze peptidyl-tRNA via the GGQ motif on ribosomes stalled by both nonstop mRNAs and mRNAs containing rare codon clusters that extend downstream from the P-site.¹⁶ It was also found that YaeJ is associated with 70S ribosomes and that the ribosome binding involves the C-terminal basic residue-rich extension following the GGQ domain.^{16,17} These findings indicate the ICT1/YaeJ protein plays a role in the rescue of stalled ribosomes during elongation of translation.

Interestingly, overexpression of ICT1, but not mtRF1a, in fibroblasts from patients lacking the C12orf65 protein resulted in approximately a 1.5-fold increase in COX activity over that in the patient fibroblasts, although the COX activity was partially recovered (60% of the control).⁴ Correspondingly, the assembly of COX was increased to some extent in the fibroblasts from patients. The partial recovery of COX activity suggests that C12orf65 and ICT1 have similar and overlapping functions. However, whereas ICT1 shows codon-independent PTH activity in an *in vitro* assay with *E. coli* 70S ribosomes,¹⁴ C12orf65 does not show any PTH activity in the presence, or in the absence, of any codon, although it is possible that C12orf65 does in fact have such an activity but that it requires 55S mitoribosomes or additional factors or that it is ribosome-independent.⁴ In addition, unlike ICT1, no interactions of C12orf65 with 55S mitochondrial ribosomes have been observed thus far.⁴ The precise role of C12orf65 as well as differences from that of ICT1 remain unclear.

To obtain insights into the function of C12orf65, we determined the solution structure of the GGQ domain of C12orf65 from *Mus musculus* by heteronuclear NMR methods. The GGQ domain is a truncated C12orf65 protein that lacks an N-terminal mitochondrial targeting signal and a basic residue-rich C-terminal extension. The determined structure enabled structure-based alignments and detailed structural comparisons with RF and ICT1,

showing not only similarities that would allow C12orf65 with PTH activity to enter a ribosome like RF and ICT1 but also differences that are key factors for discriminating between C12orf65 and ICT1 functions. Accordingly, a classification of RF-1 family proteins is established. Furthermore, to assess the function of C12orf65 in cells and mitochondria, we performed flow cytometry (FCM) analyses using siRNA-mediated knockdown of C12orf65 in HeLa cells. In addition, we compared effects of the knockdown on cells and mitochondria between C12orf65 and ICT1. The results show that C12orf65 is required for cell vitality and mitochondrial function as well as ICT1. Significant differences between C12orf65 and ICT1 were also observed in the range and pattern of the effects of knockdown, which could be linked to differences in functions.

MATERIALS AND METHODS

Sequence alignment data

Sequence alignments were performed with the CLUSTAL W program¹⁸ and then manually modified on the basis of the structures of ICT1, C12orf65, and RF. Accession codes used in the sequence alignment are as follows: *M. musculus* C12orf65, NP_001128189; *Rattus norvegicus* C12orf65, XP_573395.1; *Homo sapiens* C12orf65, NP_001137377.1; *Gallus gallus* C12orf65, NP_001239017; *Anolis carolinensis* C12orf65, XP_003222789; *Danio rerio* C12orf65, XP_001340041; *Tetraodon Nigroviridis* C12orf65, CAG08451; *Drosophila melanogaster* C12orf65, NP_725560.1; *Caenorhabditis elegans* C12orf65, CBY25203; *Saccharomyces cerevisiae* C12orf65, AAS56257; *E. coli* RF2, P07012; *E. coli* RF1, P07011; *M. musculus* mtRF1L, NP_780583; *R. norvegicus* mtRF1L, NP_001020894.1; *H. sapiens* mtRF1L, NP_061914.3; *G. gallus* mtRF1L, XP_419682.2; *Xenopus tropicalis* mtRF1L, XP_002936423; *D. rerio* mtRF1L, XP_001333894; *Strongylocentrotus purpuratus* mtRF1L, XP_001184371.1; *D. melanogaster* mtRF1L, P_609617.1; *C. elegans* mtRF1L, NP_500737; *S. cerevisiae* mtRF1L, P30775; *M. musculus* ICT1, NP_081005.1; *R. norvegicus* ICT1, XP_221110.3; *H. sapiens* ICT1, NP_001536; *G. gallus* ICT1, XP_420117.2; *Taeniopygia guttata* ICT1, XP_002190739; *X. tropicalis* ICT1, XP_002940027; *D. rerio* ICT1, XP_001922710.1; *D. melanogaster* ICT1, NP_609416.1; *C. elegans* ICT1, NP_498174.1; *S. cerevisiae* ICT1, NP_014527.

Protein expression and purification

The DNA encoding the region of the C12orf65 protein ranging from Ser21 to Asn124 was subcloned by PCR from a mouse full-length cDNA clone with the NIA mouse clone P070213-30. This DNA fragment was cloned into the expression vector pCR2.1 (Invitrogen) as a fusion with an N-terminal 6-His affinity tag and a TEV protease cleavage site. The ¹³C/¹⁵N-labeled fusion protein

was synthesized by the cell free protein expression system as described previously.^{19–21} The solution was first adsorbed to a HiTrap Chelating column (GE Healthcare), which was washed with buffer A (50 mM sodium phosphate buffer (pH 8.0) containing 500 mM sodium chloride and 20 mM imidazole) and eluted with buffer B (50 mM sodium phosphate buffer (pH 8.0) containing 500 mM sodium chloride and 500 mM imidazole). To remove the His-tag, the eluted protein was incubated at 4°C overnight with the TEV protease. After dialysis against buffer A without imidazole, the dialysate was mixed with imidazole to a final concentration of 20 mM and was then applied to a HiTrap Chelating column, which was washed with buffer A. The flow-through fraction was dialyzed against buffer C (20 mM sodium phosphate buffer [pH 7.2] containing 1 mM DTT and a protease inhibitor cocktail (complete, EDTA-free (Roche))). The dialysate was applied to a HiTrap SP column with a concentration gradient of buffer C and buffer D (20 mM sodium phosphate buffer [pH 7.2] containing 1M sodium chloride, 1 mM DTT, and the inhibitor cocktail). The C12orf65-containing fractions were collected.

For NMR measurements, the purified protein (purity: >95% by SDS-PAGE) was concentrated to ~1.0 mM in ¹H₂O/²H₂O (9:1), 20 mM Tris-*d*₁₁-HCl buffer (pH 7.0), 100 mM NaCl, 1 mM 1,4-*D,L*-dithiothreitol-*d*₁₀ (*d*-DTT), and 0.02% Na₃N.

NMR spectroscopy, structure determination, and structure analysis

All NMR measurements were performed at 23°C on a Bruker AVANCE 600 spectrometer equipped with a triple-resonance CryoProbe and an AVANCE 900 spectrometer. Sequence-specific backbone chemical shift assignments²² were made with the ¹³C/¹⁵N-labeled sample, using standard triple-resonance experiments.^{23,24} Assignments of side chains were obtained from HBHA(CO)NH, HC(CO)NH, C(CO)NH, HC(C)H-TOCSY, and HC(C)H-COSY spectra. ¹⁵N- and ¹³C-edited NOESY spectra with 80 ms mixing time were used to obtain distance restraints. The spectra were processed with the program NMRpipe.²⁵ The program KUIJIRA, which was created on the basis of NMRView,²⁶ was employed for spectral visualization and analysis.²⁷

Automated NOE cross-peak assignments^{28,29} and structure calculations with torsion angle dynamics³⁰ were performed using the software package CYANA 2.0.³¹ Peak lists of the two NOESY spectra were generated as input with the program NMRView. The input further contained the chemical shift list corresponding to the sequence-specific assignments. Dihedral angle restraints were derived using the program TALOS.³² No hydrogen bond restraints were used.

A total of 100 conformers were calculated independently. The 20 conformers with the lowest final CYANA

target function values were energy-minimized in a water shell with the program OPALp,³³ using the AMBER force field.³⁴ The structures were validated using PROCHECK-NMR.³⁵ The program MOLMOL³⁶ was used to analyze the resulting 20 conformers and to prepare drawings of the structures.

The sequence-specific resonance assignments of C12orf65 have been deposited in BioMagResBank (Accession number 11491). The atomic coordinates of the 20 energy-minimized CYANA conformers of the mouse C12orf65 protein have been deposited in the RCSB Protein Data Bank under the PDB accession code 2RSM.

Cell culture

Human HeLa cells were maintained in Dulbecco's modified Eagle's medium (DMEM) (Wako) supplemented with 10% fetal bovine serum (FBS) (GIBCO), 1 g/L glucose, 4 mM glutamine, 100 units/mL penicillin, and 100 µg/mL streptomycin at 37°C in 5% CO₂.

Preparation of siRNA

The siRNA sequence used for the targeted silencing of the c12orf65 gene was chosen as recommended by Cosmo Bio Co., Ltd., and the RNA was synthesized by Hokkaido System Science. The corresponding target mRNA sequences for the siRNAs were as follows:

si-C12orf65-A, 5-CCAGAAGCUCCAGGGAAU-3-;
si-C12orf65-B, 5-GAGAAGCGGCGAAGAAAA-3-;
si-C12orf65-C, 5-GCACUAAACUGUAGUGAAC-3-.

Nontarget duplex siRNAs (si-NT) (siTrio negative control) were purchased from Cosmo Bio Co. The corresponding target mRNA sequences used for the targeted silencing of ICT1 as well as the sequence of the nontarget duplex siRNAs have been described previously.¹⁵

Transfection

Transfection was performed by the reverse transfection method as follows. Cells were harvested by incubation with 0.05% trypsin-EDTA (Sigma-Aldrich) for 5 min at 37°C, and trypsin was inactivated by adding complete growth medium. Cell viability was assessed by trypan blue staining (Wako) and each cell suspension was incubated at 37°C in polypropylene tubes until used in the reverse transfection. siRNAs and transfection reagent HilyMax (Dojindo) were diluted in DMEM without serum and incubated for 15 min at room temperature to allow siRNAs-HilyMax complex formation. After incubation, HeLa cells (1.0×10^5 cells/well) were seeded in a 35-mm dish simultaneously with addition of the mixture complexes. The dishes were incubated at 37°C in a CO₂ incubator and 16 h after transfection, the medium in the dishes was changed to DMEM supplemented with 10% FBS and antibiotics. The final concentration of siRNAs was 50 nM.

Immunoblot assay

HeLa cells were harvested and lysed in ice-cold lysis buffer (7M urea, 2M thiourea, 1% triton X-100). Total protein concentrations of the lysate were determined using Protein assay reagent (Bio-Rad). Thirty micrograms of protein was electrophoresed on 15% SDS-PAGE and transferred to a nitrocellulose membrane (Pall). The blots were probed with a mouse polyclonal antibody against human C12orf65 (Abnova, 1:500) and a mouse monoclonal antibody against human γ -tubulin (Sigma-Aldrich, 1:4000), using Can Get Signal immunostain (Toyobo), and were successively incubated with horseradish-peroxidase-conjugated goat anti-mouse IgG antibody (Cell Signaling Technology, 1:4000). Signals were detected using the SuperSignal West Pico Chemiluminescent Substrate (ThermoFisher Scientific) according to the manufacturer's protocol. The protocol for the human ICT1 polyclonal antibody is according to Handa *et al.*¹⁵

Cell concentration

Cells were cultured in DMEM with 10% FBS in 5% CO₂ at 37°C. The cells were seeded in 35-mm dishes at a density of 1.0×10^5 per mL. Cell numbers were maintained for 0, 48, 72, and 96 h after reverse transfection to determine their growth curves. Cells were harvested by trypsinization, and cell count and viability were determined by trypan blue staining using a hemocytometer.

Annexin V-fluorescein isothiocyanate (FITC)/propidium iodide (PI) assay

To identify apoptotic cells, we stained the cells with PI and FITC-conjugated annexin V using the Annexin V-FITC Apoptosis Detection Kit I (Becton Dickinson). Annexin V indicates early apoptotic cells based on externalized phosphatidylserine. PI detects cells that have lost plasma membrane integrity (i.e., necrotic or late apoptotic cells). HeLa cells were harvested using trypsin-EDTA, washed with PBS, resuspended in 500 μ L of binding buffer supplemented with 5 μ L of annexin V-FITC and 5 μ L of PI solution, and treated in the dark for 5 min at room temperature. After the addition of binding buffer, the stained cells were kept on ice and were analyzed by FCM. We collected the FITC fluorescence at 520 nm and the PI fluorescence at 620 nm. A total of 10^4 cells per sample were measured in each experiment.

Fluorescent detection of mitochondrial membrane potential and mitochondrial mass

The membrane-potential-dependent stain MitoTracker Red CMXRos (Molecular Probes) was used to assess mitochondrial membrane potential in HeLa cells, and the green-fluorescent mitochondrial stain MitoTracker Green FM (Molecular Probes) was used to measure the mitochondria mass per cell. The cells were incubated in media

containing either stain at a final concentration of 1 μ M in 5% CO₂ at 37°C for 1 h. The cells were collected using trypsin-EDTA, resuspended in DMEM, washed with PBS, and fixed in a solution of 70% ethanol for 2 h at 4°C. The cells were analyzed by FCM.

Reactive oxygen species (ROS) measurement

Intracellular ROS accumulation was measured by FCM using the fluorescent probe 2', 7'-dichlorofluorescein diacetate (DCFH-DA). Cells treated with si-RNAs for 4 days were incubated with 10 μ M of DCFH-DA (Sigma-Aldrich) for 60 min at 37°C in the dark. As a positive control, cells without any treatment for 4 days were incubated with 10 μ M of DCFH-DA for 40 min and then with 1 mM H₂O₂ for 20 min. After incubation, the cells were detached by trypsinization, washed in PBS, suspended in PBS, and immediately analyzed by FCM to determine the DCF fluorescence intensity at excitation and emission wavelengths of 488 nm and 525 nm, respectively.

Cytochrome c oxidase assay

The cytochrome c oxidase assay was conducted using the Mitochondria Isolation Kit for Cultured Cells (PIERCE) and the cytochrome c oxidase activity assay kit (BioChain) according to the manufacturers' instructions.

RESULTS

Protein expression

The protein encoded by the mouse C12orf65 gene is composed of 184 residues.⁴ Based on the NMR structure of ICT1,¹⁵ we designed a truncated protein composed of 104 residues (Ser21-Asn124). It lacks the N-terminal region ranging from the first residue to residue 20, which is a part of an import signal into mitochondria (for human C12orf65, the signal is estimated to range from the first residue to residue 35 by the MEROPS database³⁷), and the C-terminal region ranging from residue 125 to the last residue, which abounds in basic residues (Fig. 1). ¹⁵N- and ¹³C/¹⁵N-labeled protein samples for NMR measurements were prepared by a cell-free protein expression system.^{20,21} The expressed protein consequently has artificial tag-derived sequences (11 residues in total) at the N-terminus (GSSGS) and the C-terminus (SGPSSG), which are both derived from the expression vector. The resulting truncated protein composed of 115 residues exhibited well-dispersed resonances (Supporting Information Fig. S1).

Resonance assignments and structure determination

For the structure determination of the truncated and tagged version of the C12orf65 protein, which corresponds

Table I

Summary of Conformational Constraints and Statistics of the NMR Solution Structure of the Mouse C12orf65 Protein

NOE upper distance restraints	
Intraresidual ($ i - j = 0$)	457
Medium-range ($1 \leq i - j \leq 4$)	708
Long-range ($ i - j > 4$)	280
Total	1445
Dihedral angle restraints (ϕ and ψ)	
	88
CYANA target function value (\AA^2)	1.53 ± 0.53
No. restraint violations	
Distance restraint violations ($>0.30 \text{\AA}$)	0
Dihedral angle restraint violations ($>5.0^\circ$)	0
AMBER energies (kcal/mol)	
Total	-3975 ± 107
van der Waals	-159 ± 10
Electrostatic	-4626 ± 114
RMSD from ideal geometry	
Bond length (\AA)	0.0142 ± 0.0001
Bond angles ($^\circ$)	1.85 ± 0.04
Ramachandran plot (%)	
Residues in most favored regions	81.4
Residues in additional allowed regions	17.3
Residues in generously allowed regions	1.2
Residues in disallowed regions	0.2
RMSD deviation from the averaged coordinates (\AA) (res. 49–52, 7–83, 89–108)	
Backbone atoms	0.37 ± 0.07
Heavy atoms	0.86 ± 0.07

to the GGQ domain, NMR resonances were assigned using conventional heteronuclear methods with the $^{13}\text{C}/^{15}\text{N}$ -labeled protein composed of 115 residues. The assignments of backbone resonances were 93% complete for all residues except those in the region of the tag sequences. Residues with an unassigned backbone are Gly22, Lys23 His71, Gln76, Asn79, Ser82, Asn83, His99, Arg102, and Val104. Tertiary structures were calculated using the CYANA software package,^{28,30} based on a total of 1445 NOE-derived distance restraints and 88 backbone torsion angle restraints (Table I). A best-fit superposition of the ensemble of the 20 lowest-energy conformers is shown in Figure 2(A). The root mean square deviation (RMSD) from the mean structure was $0.37 \pm 0.07 \text{\AA}$ for the backbone (N, C^α , C') atoms $0.86 \pm 0.07 \text{\AA}$ for all heavy (nonhydrogen) atoms in the well-ordered region of residues 49–52, 70–83, and 89–108. The statistics of the structures are summarized in Table I.

The NMR results show that the structure consists of a three-stranded antiparallel β -sheet side by side with an α -helix, with the topology of 3_{10} - $\beta 1$ - $\beta 2$ - $\beta 3$ - $\alpha 1$ (Fig. 2B). The β -sheet consists of three antiparallel β -strands ($\beta 1$: 64–68, $\beta 2$: 84–88, $\beta 3$: 95–98). A 3_{10} -helical turn (60–62) precedes $\beta 1$. The strands $\beta 1$ and $\beta 2$ are connected by a disordered loop (69–83) including the $^{74}\text{GGQ}^{76}$ residues, which is termed the GGQ loop. The strands $\beta 2$ and $\beta 3$ are connected by a six-residue turn, as described below. Following $\beta 3$, a long α -helix ($\alpha 1$: 104–124) lies on the β -sheet. The N-terminal region (55–59) followed by the 3_{10} -helical turn including three Leu residues (55, 56, and

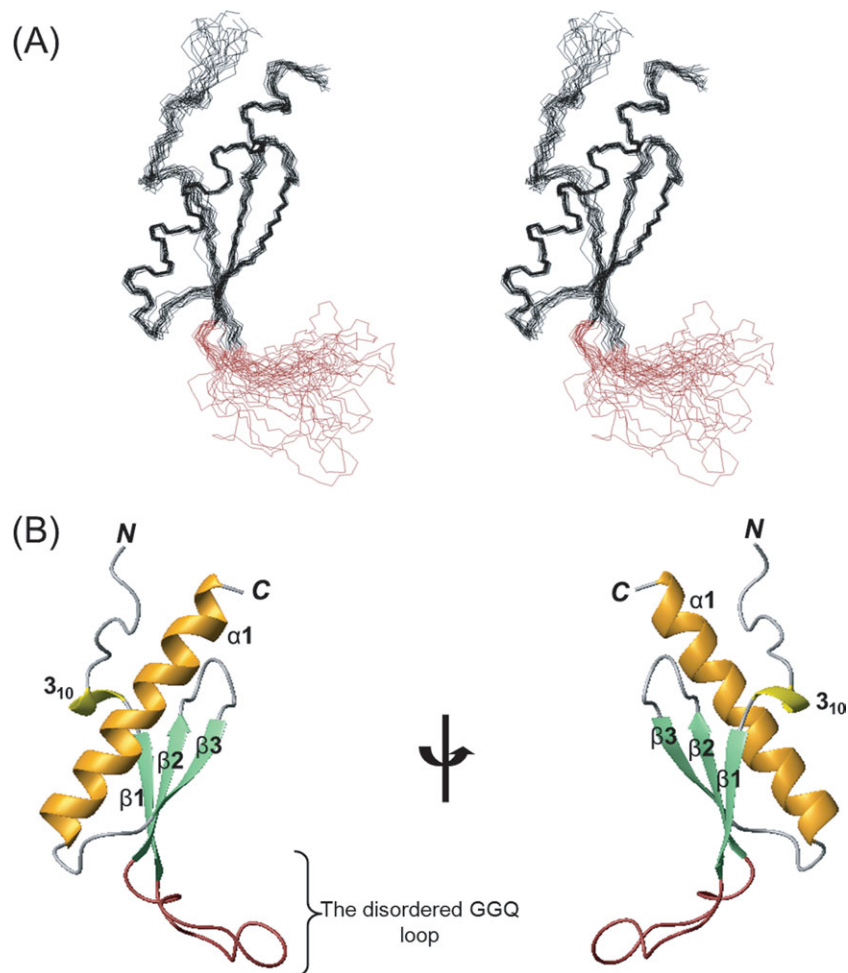
58) interact with $\alpha 1$ and are thus ordered [Fig. 3(A)]. As a result, the structured region of the C12orf65 protein ranges from Leu55 to Asn124. No long-range distance restraints from any of the residues except for those in the structured region were observed (Supporting Information Fig. 2S).

Structural comparison with ICT1 and domain 3 of bacterial-type RF

Figure 3 shows three structures of the GGQ domains of C12orf65, ICT1, and bacterial-type RF (domain 3 of *E. coli* RF2). A comparison of the three structures showed that the GGQ domains have essentially the same structural framework with a 3_{10} - $\beta 1$ - $\beta 2$ - $\beta 3$ - $\alpha 1$ topology [Fig. 3(D)]. The RMSD between the GGQ domains of C12orf65 and RF is 0.77\AA for the backbone atoms in the region including the three-stranded β -sheet and the long α -helix [Fig. 3(E)], and that between the GGQ domains of C12orf65 and ICT1 is 1.1\AA [Fig. 3(F)]. The GGQ domains of C12orf65 and RF are identical in not only the structural framework but also the number of residues forming the 3_{10} helix, β -strands, and linking loops, and thus differ only in the length of the α -helix, $\alpha 1$ [Figs. 1 and 3(E)].

The GGQ loop connecting $\beta 1$ and $\beta 2$ is the same in the three proteins in terms of location and length (15 residues) [Fig. 3(E,F)]. In the solution structures, the GGQ loop appears to be unstructured [Fig. 2(A) and Supporting Information Fig. S2]. This loop property is also seen in the GGQ domains of free RF and ICT1.^{16,38} The GGQ loop of bound RF adopts a fixed conformation, with the GGQ motif residues contributing directly to PTH activity.^{10,11} The loop sequence is 40% identical and 53% similar between C12orf65 and mtRF from humans (Fig. 1). In addition, the conformation of the structured $\beta 3/\alpha 1$ loop in the vicinity of the GGQ loop is virtually identical in the three proteins, where one Arg residue (Arg87 in C12orf65) is conserved among them in all species [Figs. 1 and 3(D)].

The only difference in the structural framework of the GGQ domain among the three proteins is in the region connecting $\beta 2$ and $\beta 3$, where C12orf65 and RF have a six-residue turn, whereas ICT1 has a 10-residue α -helix, α_i , sandwiched between the β -sheet and $\alpha 1$ (Fig. 3). In C12orf65 and RF, the turn connecting $\beta 2$ and $\beta 3$ is always composed of six residues, and the sequence is highly conserved in all species ($^{89}\text{H}-(\text{L}/\text{V}/\text{I})-\text{P}-(\text{S}/\text{T})-\text{G}-(\text{I}/\text{V}/\text{L})^{94}$) (Fig. 1 and Supporting Information Fig. S3). According to the Ramachandran nomenclature,³⁹ this region adopts a β - α - α - α - α_L - β conformation, such that this turn can be classified as a π -HB turn, one of the two major classes of six-residue π -turns (for π -HB turns, the α - α - α - α_L conformation being most frequent).⁴⁰ In light of the structures of C12orf65 and domain 3 of RF2, most of the conserved His residue is buried inside the

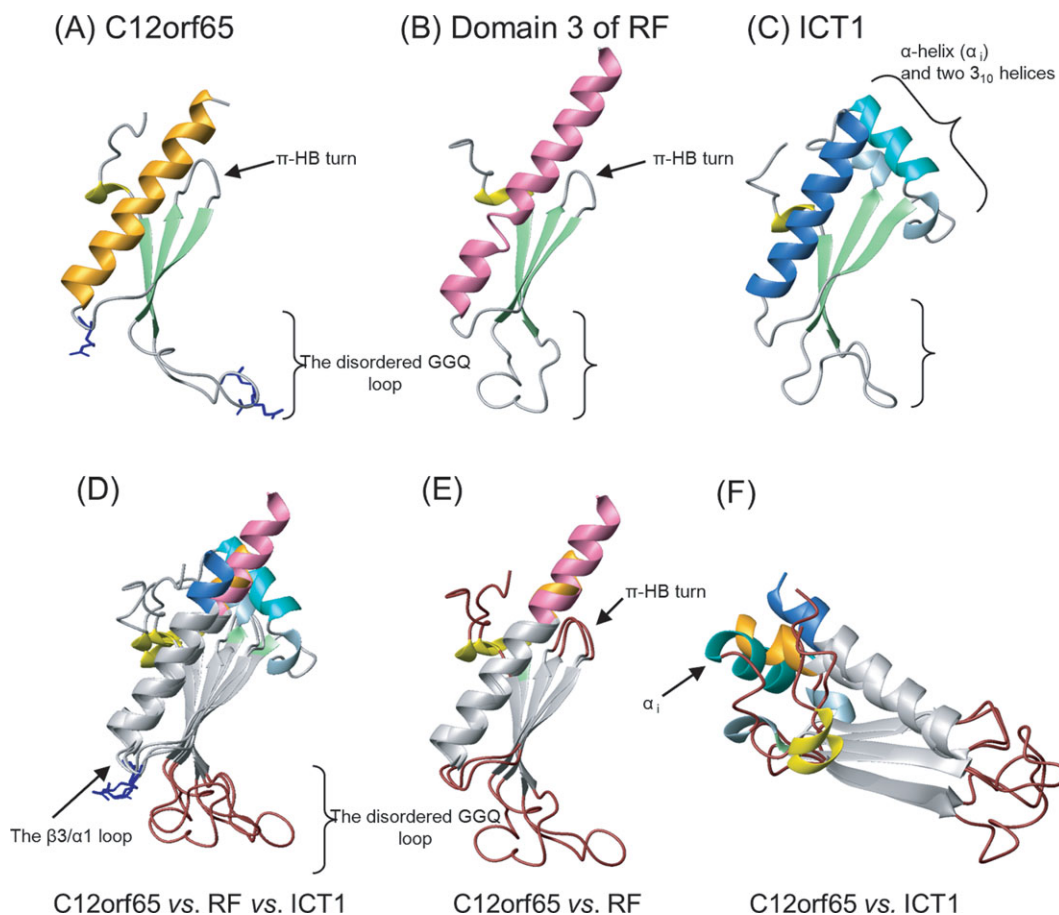
**Figure 2**

Solution structure of the GGQ domain of the C12orf65 protein. (A) Stereo view illustrating a trace of the backbone atoms of the 20 energy-refined conformers that represent the solution structure (residues 52–125). Disordered regions at both termini are omitted. The GGQ loop is shown in brown. (B) Ribbon diagrams of the structure of the C12orf65 GGQ domain. The orientation in the left view is the same as that in (A). On the right, the view is rotated by 180° around a vertical axis. The α -helix, 3_{10} helix, β -strands, and GGQ loop are colored orange, yellow, light green, and brown, respectively.

structures, and the N ^{$\delta 1$} proton of the His side chain appears to form a hydrogen bond with the hydroxyl group of the semiconserved Ser/Thr residue, contributing to the structural stability of the turn. Besides, three residues on the internal side of the π -HB turn (His89, Ser92, and Ile94) interact with five residues on the internal side of the C-terminal part of $\alpha 1$ (Leu115, Lys118, Val119, Phe122, and Tyr123), all of which are well conserved (Fig. 1 and Supporting Information Fig. S3). The conservation of the π -HB turn is probably involved in the maintenance of stable interactions with $\alpha 1$. Instead of the π -HB turn, in ICT1, the sandwiched characteristic α -helical region, α_i , occurs among all species, interacting with $\alpha 1$ [Fig. 3(F)]. In α_i , a few positively charged residues are well conserved and are thought to be involved in an interaction with protein and/or RNA in the ribosome.¹⁶

Flow cytometry analysis using siRNA-mediated knockdown of C12orf65

To assess C12orf65 function in cells and mitochondria, we downregulated C12orf65 expression in HeLa cells using siRNA methods. Cells transfected with nontargeting siRNA (si-NT) served as negative controls. The siRNA used, si-C12orf65, was efficient in the knockdown of C12orf65 from cells [Fig. 4(A)]. For comparison, we also downregulated ICT1 expression using siRNA methods as described previously.¹⁵ Quantitative PCR analysis confirmed that transfection of si-C12orf65 or si-ICT1 curtails their respective mRNA without influencing other mRNA levels (Supporting Information Fig. S4). Four days after the addition of siRNA, a 64% reduction in cell numbers was observed in the C12orf65-downregulated cells compared with the si-NT control cells, indicating

**Figure 3**

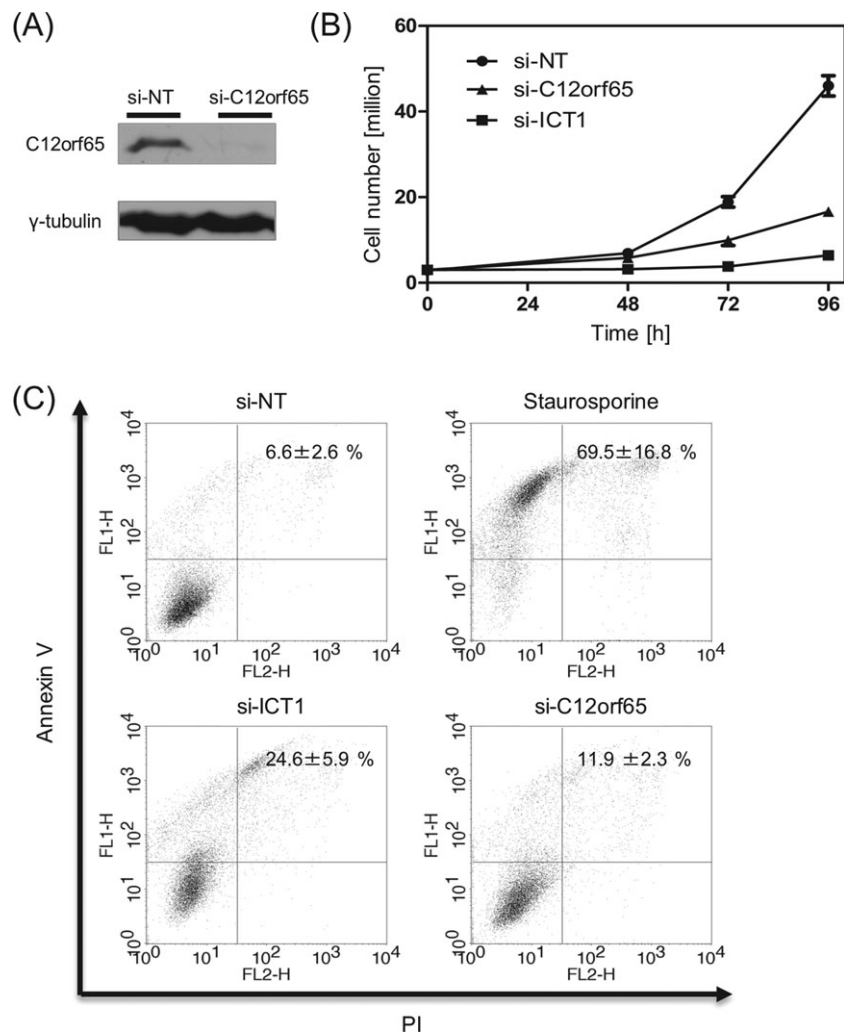
Comparison of three structures of the GGQ domains in RF-1 family proteins. The top panel shows ribbon diagrams of structures of the C12orf65 GGQ domain (residues 54–125) (A), domain 3 of free *E. coli* RF2 (230–307) (1GQE) (B), and ICT1 GGQ domain (68–163) (1J26) (C). In C12orf65, RF domain 3, and ICT1, the last α -helix following $\beta 3$ is colored orange, pink, and dark blue, respectively. Only ICT1 has an α -helix, α_1 , (turquoise) and two 3_{10} helices (light blue) linking $\beta 2$ and $\beta 3$ instead of a π -HB turn. The GGQ motif residues (Gly74, Gly75, and Gln76) and Arg102 in the $\beta 3/\alpha 1$ loop that are conserved among the three proteins are indicated in blue. Note that the N-terminal region followed by the 3_{10} helix is ordered in the three structures. The bottom panel shows superpositions of the ribbon diagrams of the three GGQ domain structures (D), those of C12orf65 versus RF domain 3 (E), and those of C12orf65 versus ICT1 (F). Shown in gray are the regions used for determining the optimal superposition: residues 64–68, 84–89, 94–98, and 104–118 in C12orf65; 78–82, 98–103, 133–137, and 143–157 in ICT1; and 240–244, 260–265, 270–274, and 280–294 in RF domain 3.

inhibition of cell proliferation [Fig. 4(B)]. Comparison with the ICT1-downregulated cells showed that the inhibitory effect of the lack of ICT1 on cell vitality is greater than the inhibitory effect of the lack of C12orf65.

To further examine the effects of the lack of C12orf65 on cell proliferation, we performed flow cytometry (FCM) analyses of C12orf65-downregulated cells. First, to analyze the cell cycle profile, we stained C12orf65-downregulated cells with propidium iodide (PI) after 4 days treatment, and we counted the number of cells in each phase by FCM. The FCM analysis showed that 13% of the C12orf65-downregulated cells were accumulated in the sub- G_1 phase in contrast to 6.5% of the si-NT control cells, indicating that apoptosis occurred in the cells (Supporting Information Fig. S5). Annexin V and PI stainings were also performed to confirm apoptotic cell

death. This staining combination enables viable, apoptotic, and necrotic cells to be distinguished.⁴¹ As shown in Figure 4(C), 11.9% of the C12orf65-downregulated cells were apoptotic, while only 6.6% of the si-NT control cells were apoptotic. These results indicate that the lack of C12orf65 results in apoptotic cell death. The percentage of apoptotic cells in ICT1-downregulated cells was almost twice that in C12orf65-downregulated cells.

Apoptosis is often linked to the generation of reactive oxygen species (ROS) that mainly occurs in mitochondria.⁴² To confirm intracellular ROS generation of C12orf65-downregulated cells, we measured ROS levels by FCM using the oxidation-sensitive probe 2',7'-dichlorofluorescein diacetate (DCFH-DA). The ROS level in C12orf65-downregulated cells was 1.2-fold higher than that in control cells, whereas that in ICT1-downregulated

**Figure 4**

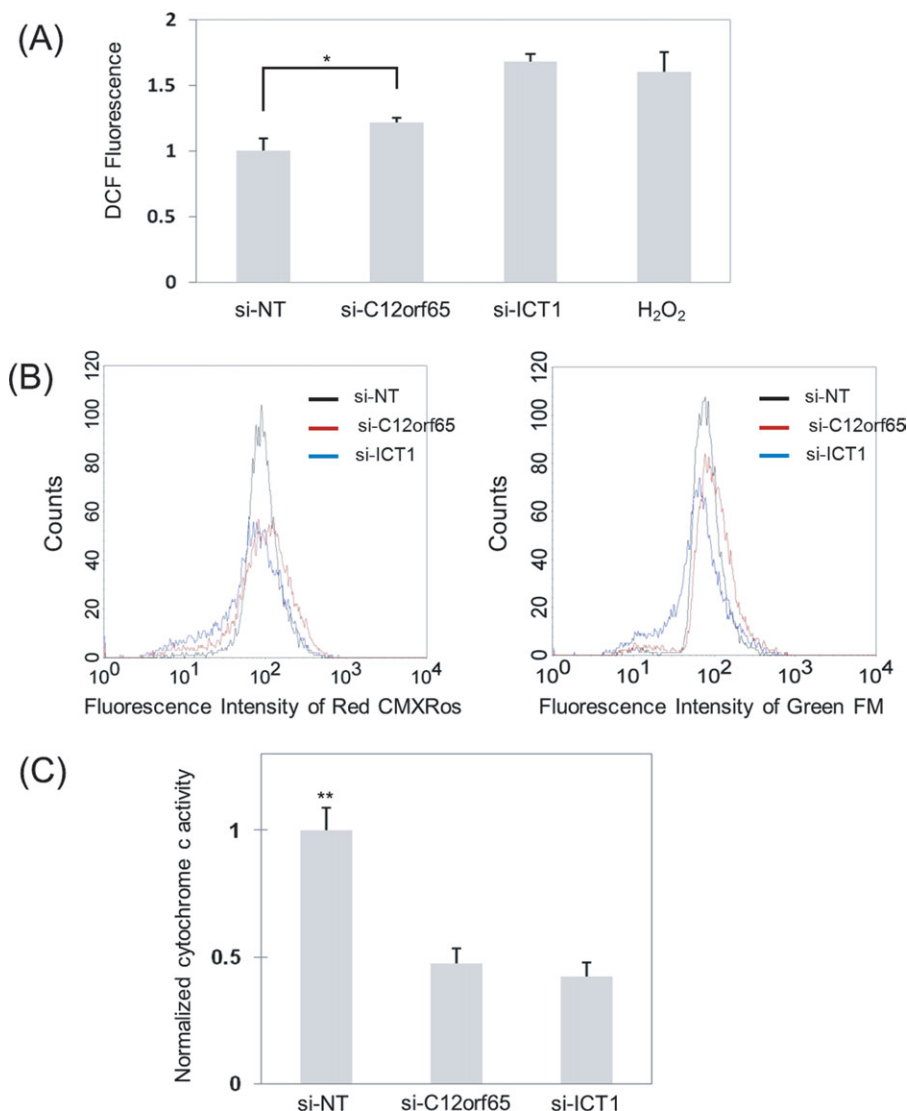
Apoptotic cell death in C12orf65-downregulated HeLa cells. (A) Immunoblot analysis showing C12orf65 and γ -tubulin protein levels in HeLa cells harvested from a 2-day experiment. (B) Numbers counted at 1-day intervals of HeLa cells in standard glucose media. HeLa cells were transfected with nontargeting control (si-NT), si-C12orf65, or si-ICT1. Data points show the mean of three independent experiments; bars indicate the standard deviation. (C) Scatterplots of FCM determination of the numbers of apoptotic, necrotic, and viable cells using PI versus annexin V. HeLa cells were transfected with si-NT, si-C12orf65, or si-ICT1 or treated with 1 nmol of an apoptotic inducer, staurosporine, and grown for 4 days. Cells were labeled with PI and annexin V and analyzed by FCM. Numbers indicate the percentage of early apoptotic cells localized in the upper left quadrant of a scatterplot graph. Each value is the mean \pm standard deviation of three independent experiments.

cells was increased by 1.7-fold, comparable to that in H_2O_2 -treated positive control cells [Fig. 5(A)].

Furthermore, to characterize mitochondrial properties in C12orf65-downregulated cells, we measured changes in mitochondrial membrane potential and mass in C12orf65-downregulated cells by FCM analysis using the uptake of Red CMXRos and MitoTracker Green FM, respectively. Uptake of the former dye is dependent on mitochondrial potential but not mass, whereas uptake of the latter dye is dependent on mass but not mitochondrial potential. Significant decreases of peak counts in fluorescent detections of both mitochondrial membrane potential and mass were found in C12orf65-downregu-

lated cells compared with those in control cells [Fig. 5(B)]. Although similar decreases of peak counts in ICT1-downregulated cells were observed, the directions of peak shifts in fluorescent detections of mitochondrial membrane potential and mass differ from those in ICT1-downregulated cells.

In addition, a cytochrome c oxidase activity assay was performed in an isolated mitochondrial fraction from C12orf65-downregulated cells. The activity of cytochrome c oxidase was decreased by 52% compared with that in control cells [Fig. 5(C)]. The results indicated dysfunction of mitochondria in C12orf65-downregulated cells. A similar decrease was observed in ICT1-downregulated cells.

**Figure 5**

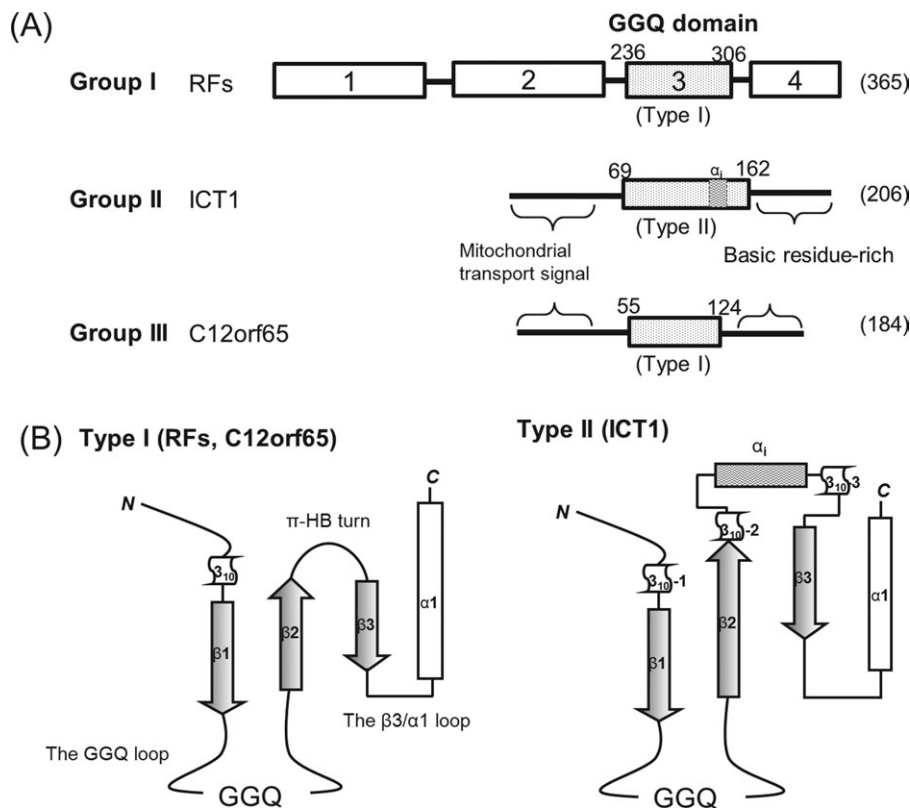
Effects of knockdown of C12orf65 on mitochondria. (A) Intracellular ROS production induced by C12orf65 and ICT1 knockdown. Four days after transfection, the level of intracellular ROS was monitored using DCF fluorescence by FCM. H₂O₂-treated cells (1 mM) were used as positive controls. Each value is the mean ± standard deviation of three independent experiments. **p* < 0.05. (B) Mitochondrial membrane potential (left) and mass (right) measured by FCM using MitoTracker Red CMXRos and MitoTracker Green FM, respectively. HeLa cells were transfected with si-NT, si-C12orf65, or si-ICT1, and grown for 4 days. (C) Cytochrome c oxidase activity. Each value is the mean ± standard deviation of three independent experiments. ***p* < 0.01.

These findings showed that the lack of C12orf65 has severe effects on cell vitality and mitochondrial functions. The findings also revealed that the effects are less significant in C12orf65-downregulated cells than in ICT1-downregulated cells.

DISCUSSION

In this study, we determined the solution structure of the GGQ domain of the eukaryotic C12orf65 protein. Structural comparison showed that the GGQ domain of

C12orf65 has a virtually identical structural framework as those of RF and ICT1 (Fig. 3). Considering the similarities in sequence including the GGQ motif, the GGQ domain of C12orf65 presumably has PTH activity on the mitoribosome via the GGQ motif as an active site. This assumption is supported by the success of overexpression of ICT1 in partially recovering the decrease in COX activity in C12orf65-defective cells.⁴² Furthermore, all three structures of the GGQ domain allowed a comprehensive structure-based alignment of RF-1 family proteins, which are all characterized by the presence of a GGQ motif

**Figure 6**

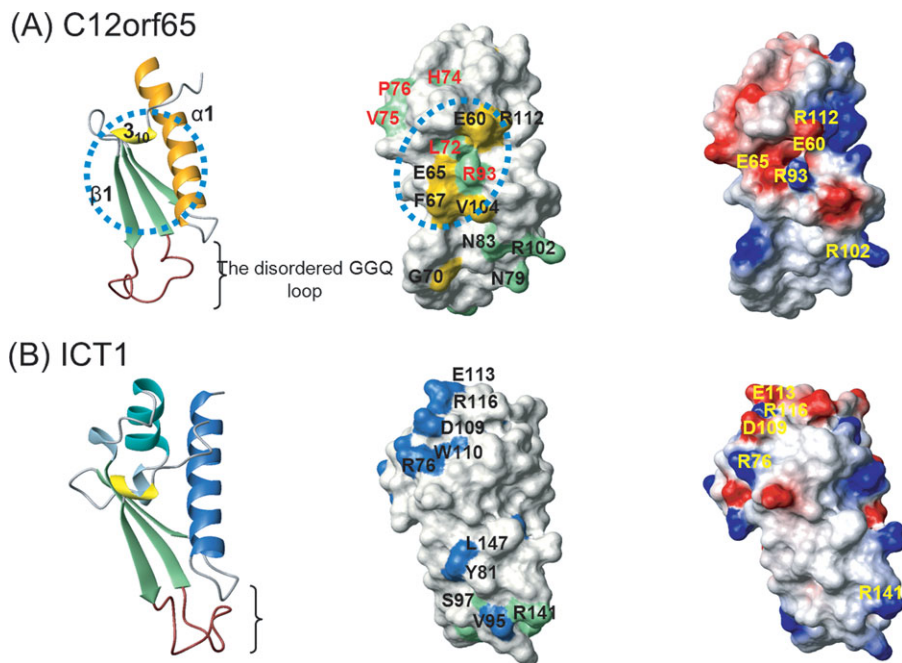
Classification of RF-1 family proteins. (A) Schematic domain representations of three groups of RF-1 family proteins. Numbers in parentheses indicate residues of each protein. (B) Topology of two types of GGQ domain structures.

(Fig. 1). Accordingly, it was revealed that RF-1 family proteins can be divided into three groups, depending on amino acid sequence, while the GGQ domains can be divided into two types, depending on structure (Fig. 6). Thus, most eukaryotic cells have three groups of proteins: mtRF, ICT1, and C12orf65, all of which are located in mitochondria. However, vertebrate mitochondria have not only a classical RF (mtRF1a/HMRF1L) but also a second RF-homolog (mtRF1/HMRF1), of which the function remains elusive, although the GGQ domains are quite similar.⁴³

To gain an insight into the function of the GGQ domain of C12orf65 and clarify differences in function between C12orf65 and ICT1, we mapped putative functional residues on the structures that are highly conserved among each protein across eukaryotes but do not appear among mitochondrial RFs. We also identified surface clusters that may play a functional role. Two clusters of C12orf65-specific conserved residues were found on the surface of the C12orf65 structure [Fig. 7(A) and Supporting Information Fig. S6). Cluster 1 is composed of Glu60 in β_{10} , Glu65 in β 1, Phe67 in β 1, Val104 in α 1, and Arg112 in α 1, and cluster 2 is composed of Val68 in β 1, Lys97 in β 3, and His99 in the β 3/ α 1 loop. In addition,

comparison of the putative functional residues between C12orf65 and ICT1 highlighted differences in the positions of the protein-specific clusters and surface electrostatic charge distribution (Fig. 7). The differences are most likely linked to not only those of a ribosome binding mode but also to those of a role in ribosome rescue.

In the C-terminal region, instead of a structured domain in RF that recognizes the stop codon, both C12orf65 and ICT1 have a characteristic basic residue-rich region composed of ~ 20 residues following the last α -helix (Fig. 1). However, no consensus sequence can be found in this region between C12orf65 and ICT1, except for the abundance of basic residues. Since in the *E. coli* ICT1 homolog, YaeJ, deletion of the C-terminal region results in the loss of ribosome binding,^{16,17} the C-terminal region of ICT1 could also be directly involved in ribosome binding. Very recently, a crystal structure of YaeJ bound to the *Thermus thermophilus* 70S ribosome in complex with the initiator tRNA^{Met} and a short mRNA has been reported, revealing that the C-terminal tail of YaeJ functions as a sensor to discriminate between stalled and actively translating ribosomes by binding in the mRNA entry channel downstream of the A site.⁴⁴ However, unlike ICT1, no interactions between C12orf65

**Figure 7**

Surface representations of the GGQ domain structure of C12orf65 (A) and ICT1 (B) showing the side chains of highly conserved residues, and the electrostatic potential. The ribbon diagrams (left) and surface representations (middle and right) are shown in the same orientation. In the middle representation, highly conserved residues among only C12orf65 proteins from eukaryotes (>90%; indicated by the code † colored in red in Fig. 1) and those among both C12orf65 proteins and mtRFs (>90%; indicated by the code ‡ colored in black in Fig. 1) are depicted in yellow and light green, respectively (A). Highly conserved residues among only ICT1 proteins from eukaryotes and those among both ICT1 proteins and mtRFs are depicted in blue and light green, respectively (B). Note that the GGQ loops are disordered in both structures and thus their shapes vary. Cluster 1 is indicated by a blue dotted line, as described in the text. The right representations show electrostatic potentials (blue, positive; red, negative) calculated by MOLMOL.³⁶

and mitoribosomes have been detected thus far, suggesting that C12orf65 is free in the mitochondrial matrix.⁴ It is possible that C12orf65 may bind to a specific stalled or troubled ribosome only when the C-terminal region of C12orf65 becomes accessible. In contrast, considering that ICT1 is always associated with ribosomes,¹⁴ during normal translation elongation and termination, ICT1 is thought to be positioned away from the A-site so as not to disturb the entry of aminoacyl-tRNAs or RFs. Only when a ribosome is stalled, the position of ICT1 could be altered to enter the A-site of the stalled ribosome to hydrolyze a peptidyl-tRNA at the P-site. Whether C12orf65 or ICT1 rescues stalled ribosomes seems to depend on the conditions of stalled ribosomes or kinds of translating genes, as described below.

FCM analysis showed that the lack of C12orf65 in HeLa cells results in ROS production and apoptotic cell death, leading to the inhibition of cell proliferation. In addition, FCM analysis showed significant profile changes in mitochondrial membrane potential and mass, and cytochrome c oxidase activity was impaired. These mitochondrial dysfunctions are consistent with a significant decrease of OXPHOS complexes in fibroblasts from patients.⁴ The lack of C12orf65 probably results in subu-

nits of the complexes coding for 13 genes (in mammals) of mtDNA not being synthesized sufficiently. Consequently, accumulation of these defective mitochondria would lead to increased ROS production and apoptosis. A series of consequences of the deficiency of C12orf65 may be associated with mitochondrial diseases in patients with loss of function of C12orf65.

A comparison of the results for C12orf65- and ICT1-downregulated cells shows differences in the range and patterns of effects on mitochondrial functions. Inhibitory effects on cell proliferation, the ratio of apoptotic cell death, and the increase of ROS level are less in C12orf65-downregulated cells than in ICT1-downregulated cells. It appears that ICT1 plays a wider range of roles in ribosome rescue than does C12orf65. In addition, although both C12orf65 and ICT1 downregulations resulted in large decreases of cells that have normal mitochondria, the directions of peak shifts in fluorescent detections of the mitochondrial membrane potential and mass differ between C12orf65- and ICT1-downregulated cells [Fig. 5(B)]. In C12orf65-downregulated cells, rightward peak shifts were observed in both fluorescent detections compared with that in control cells, indicating an increase of abnormal cells with higher mitochondrial

membrane potential and mass. An increase of mitochondrial mass has often been observed in mitochondrial myopathies and is thought to partly compensate for the dysfunction by maintaining overall ATP production.^{45,46}

On the other hand, leftward peak shifts in both fluorescent detections were observed in ICT1-downregulated cells, indicating an increase of abnormal cells showing a decrease of mitochondrial membrane potential and mass. The lack of ICT1 appears to impair the functions of mitochondria and cells so severely that mitochondrial mass cannot be increased. These differences suggest that the lack of C12orf65 or ICT1 inhibits translation of different genes or that C12orf65 and ICT1 show a different preference for ribosome rescue. Target genes for rescue or target conditions of stalled ribosomes may be different between C12orf65 and ICT1, although the roles of C12orf65 and ICT1 are partially overlapping.

Taken together, the significant effects of the lack of C12orf65 or ICT1 on mitochondria suggest that ribosome stalling or troubles occurs at high frequency during mitochondrial translation. This may explain why C12orf65 and ICT1 genes are both conserved among various eukaryotes from yeast to humans. Throughout evolution, both C12orf65 and ICT1 appear to have been essential for dealing with various types of ribosome stalling or troubles in the mitochondrial translation apparatus, which is highly specialized for the expression of membrane proteins. Intriguingly, the proteins coding for mtDNA are different in type and number among species, except for three genes (cob, cox1, and cox3).⁴⁷ It would be interesting to examine whether there are species-specific differences between C12orf65 and ICT1 functions.

Further combination of functional and structural studies would lead to a better understanding of each specific role of C12orf65 and ICT1. For example, findings of structural studies enable useful structure-based mutations of the two proteins, which can be applied to functional assays including the introduction of various structure-based mutants into knockdown cells. These studies will provide more insights into the C12orf65- and ICT1-mediated ribosome rescue systems during mitochondrial translation.

ACKNOWLEDGMENTS

Special thanks are due to Dr. Kohei Saitou, who provided the authors with motivation to begin studying the C12orf65 protein. The authors are grateful to Dr. Tsukasa Oda for his invaluable help with the FCM analysis and to Dr. Seiji Torii for critical comments. The authors also thank Ms. Mayu Enomoto for assistance in the NMR structural analysis.

REFERENCES

1. Taylor RW, Turnbull DM. Mitochondrial DNA mutations in human disease. *Nat Rev Genet* 2005;6:389–402.
2. Smits P, Smeitink J, van den Heuvel L. Mitochondrial translation and beyond: processes implicated in combined oxidative phosphorylation deficiencies. *J Biomed Biotechnol* 2010;2010:737385.
3. Debray FG, Lambert M, Mitchell GA. Disorders of mitochondrial function. *Curr Opin Pediatr* 2008;20:471–482.
4. Antonicka H, Østergaard E, Sasarman F, Weraarpachai W, Wibrand F, Pedersen AM, Rodenburg RJ, van der Knaap MS, Smeitink JA, Chrzanowska-Lightowlers ZM, Shoubridge EA. Mutations in *C12orf65* in patients with encephalomyopathy and a mitochondrial translation defect. *Am J Hum Genet* 2010;87:115–122.
5. Punta M, Cogill PC, Eberhardt RY, Mistry J, Tate J, Bournnell C, Pang N, Forslund K, Ceric G, Clements J, Heger A, Holm L, Sonnhammer EL, Eddy SR, Bateman A, Finn RD. The Pfam protein families database. *Nucleic Acids Res* 2012;40:D290–D301.
6. Klaholz BP, Pape T, Zavialov AV, Myasnikov AG, Orlova EV, Vestergaard B, Ehrenberg M, van Heel M. Structure of the *Escherichia coli* ribosomal termination complex with release factor 2. *Nature* 2003;421:90–94.
7. Rawat UB, Zavialov AV, Sengupta J, Valle M, Grassucci RA, Linde J, Vestergaard B, Ehrenberg M, Frank J. A cryo-electron microscopic study of ribosome-bound termination factor RF2. *Nature* 2003;421:87–90.
8. Zavialov AV, Mora L, Buckingham RH, Ehrenberg M. Release of peptide promoted by the GGQ motif of class 1 release factors regulates the GTPase activity of RF3. *Mol Cell* 2002;10:789–798.
9. Frolova LY, Tsvikovskii RY, Sivolobova GF, Oparina NY, Serpinsky OI, Blinov VM, Tatkov SI, Kisselev LL. Mutations in the highly conserved GGQ motif of class 1 polypeptide release factors abolish ability of human eRF1 to trigger peptidyl-tRNA hydrolysis. *RNA* 1999;5:1014–1020.
10. Laurberg M, Asahara H, Korostelev A, Zhu J, Trakhanov S, Noller HF. Structural basis for translation termination on the 70S ribosome. *Nature* 2008;454:852–857.
11. Weixlbaumer A, Jin H, Neubauer C, Voorhees RM, Petry S, Kelley AC, Ramakrishnan V. Insights into translational termination from the structure of RF2 bound to the ribosome. *Science* 2008;322:953–956.
12. Kumar A, Agarwal S, Heyman JA, Matson S, Heidtman M, Piccirillo S, Umansky L, Drawid A, Jansen R, Liu Y, Cheung KH, Miller P, Gerstein M, Roeder GS, Snyder M. Subcellular localization of the yeast proteome. *Genes Dev* 2002;16:707–719.
13. Pagliarini DJ, Calvo SE, Chang B, Sheth SA, Vafai SB, Ong SE, Walford GA, Sugiana C, Boneh A, Chen WK, Hill DE, Vidal M, Evans JG, Thorburn DR, Carr SA, Mootha VK. A mitochondrial protein compendium elucidates complex I disease biology. *Cell* 2008;134:112–123.
14. Richter R, Rorbach J, Pajak A, Smith PM, Wessels HJ, Huynen MA, Smeitink JA, Lightowlers RN, Chrzanowska-Lightowlers ZM. A functional peptidyl-tRNA hydrolase, ICT1, has been recruited into the human mitochondrial ribosome. *EMBO J* 2010;29:1116–1125.
15. Handa Y, Hikawa Y, Tochio N, Kogure H, Inoue M, Koshiba S, Güntert P, Inoue Y, Kigawa T, Yokoyama S, Nameki N. Solution structure of the catalytic domain of the mitochondrial protein ICT1 that is essential for cell vitality. *J Mol Biol* 2010;404:260–273.
16. Handa Y, Inaho N, Nameki N. YaeJ is a novel ribosome-associated protein in *Escherichia coli* that can hydrolyze peptidyl-tRNA on stalled ribosomes. *Nucleic Acids Res* 2011;39:1739–1748.
17. Chadani Y, Ono K, Kutsukake K, Abo T. *Escherichia coli* YaeJ protein mediates a novel ribosome-rescue pathway distinct from SsrA- and ArfA-mediated pathways. *Mol Microbiol* 2011;80:772–785.
18. Thompson JD, Higgins DG, Gibson TJ. CLUSTAL W: improving the sensitivity of progressive multiple sequence alignment through sequence weighting, position-specific gap penalties and weight matrix choice. *Nucleic Acids Res* 1994;22:4673–4680.
19. Kigawa T. Cell-free protein production system with the *E. coli* crude extract for determination of protein folds. *Methods Mol Biol* 2010;607:101–111.

20. Kigawa T, Yabuki T, Matsuda N, Matsuda T, Nakajima R, Tanaka A, Yokoyama S. Preparation of *Escherichia coli* cell extract for highly productive cell-free protein expression. *J Struct Funct Genomics* 2004;5:63–68.
21. Kigawa T, Yabuki T, Yoshida Y, Tsutsui M, Ito Y, Shibata T, Yokoyama S. Cell-free production and stable-isotope labeling of milligram quantities of proteins. *FEBS Lett* 1999;442:15–19.
22. Wüthrich K. *NMR of proteins and nucleic acids*. New York: John Wiley & Sons, Inc.; 1986.
23. Bax A. Multidimensional nuclear magnetic resonance methods for protein studies. *Curr Opin Struct Biol* 1994;4:738–744.
24. Cavanagh J, Fairbrother WJ, Palmer IIIAG, Skelton NJ. *Protein NMR spectroscopy, principles and practice*. San Diego: Academic Press, Inc.; 1996.
25. Delaglio F, Grzesiek S, Vuister GW, Zhu G, Pfeifer J, Bax A. NMRPipe: a multidimensional spectral processing system based on UNIX pipes. *J Biomol NMR* 1995;6:277–293.
26. Johnson B, Blevins R. NMRView: a computer program for the visualization and analysis of NMR data. *J Biomol NMR* 1994;4:603–614.
27. Kobayashi N, Iwahara J, Koshiba S, Tomizawa T, Tochio N, Güntert P, Kigawa T, Yokoyama S. KUJIRA, a package of integrated modules for systematic and interactive analysis of NMR data directed to high-throughput NMR structure studies. *J Biomol NMR* 2007;39:31–52.
28. Herrmann T, Güntert P, Wüthrich K. Protein NMR structure determination with automated NOE-identification in the NOESY spectra using the new software ATNOS. *J Biomol NMR* 2002;24:171–189.
29. Güntert P. Automated structure determination from NMR spectra. *Eur Biophys J* 2009;38:129–143.
30. Güntert P, Mumenthaler C, Wüthrich K. Torsion angle dynamics for NMR structure calculation with the new program DYANA. *J Mol Biol* 1997;273:283–298.
31. Güntert P. Automated NMR protein structure calculation. *Prog NMR Spectrosc* 2003;43:105–125.
32. Cornilescu G, Delaglio F, Bax A. Protein backbone angle restraints from searching a database for chemical shift and sequence homology. *J Biomol NMR* 1999;13:289–302.
33. Koradi R, Billeter M, Güntert P. Point-centered domain decomposition for parallel molecular dynamics simulation. *Comput Phys Commun* 2000;124:139–147.
34. Cornell WD, Cieplak P, Bayly CI, Gould IR, Merz KM, Ferguson DM, Spellmeyer DC, Fox T, Caldwell JW, Kollman PA. A second generation force field for the simulation of proteins, nucleic acids, and organic molecules. *J Am Chem Soc* 1995;117:5179–5197.
35. Laskowski RA, Rullmannn JA, MacArthur MW, Kaptein R, Thornton JM. AQUA and PROCHECK-NMR: programs for checking the quality of protein structures solved by NMR. *J Biomol NMR* 1996;8:477–486.
36. Koradi R, Billeter M, Wüthrich K. MOLMOL: a program for display and analysis of macromolecular structures. *J Mol Graph* 1996;14:51–55.
37. Rawlings ND, Barrett AJ, Bateman A. MEROPS: the database of proteolytic enzymes, their substrates and inhibitors. *Nucleic Acids Res* 2012;40:D343–D350.
38. Vestergaard B, Van LB, Andersen GR, Nyborg J, Buckingham RH, Kjeldgaard M. Bacterial polypeptide release factor RF2 is structurally distinct from eukaryotic eRF1. *Mol Cell* 2001;8:1375–1382.
39. Efimov AV. Standard structures in proteins. *Prog Biophys Mol Biol* 1993;60:201–239.
40. Dasgupta B, Chakrabarti P. pi-Turns: types, systematics and the context of their occurrence in protein structures. *BMC Struct Biol* 2008;8:39.
41. Vermes I, Haanen C, Reutelingsperger C. Flow cytometry of apoptotic cell death. *J Immunol Methods* 2000;243:167–190.
42. Orrenius S, Gogvadze V, Zhivotovsky B. Mitochondrial oxidative stress: implications for cell death. *Annu Rev Pharmacol Toxicol* 2007;47:143–183.
43. Young DJ, Edgar CD, Murphy J, Fredebohm J, Poole ES, Tate WP. Bioinformatic, structural, and functional analyses support release factor-like MTRF1 as a protein able to decode nonstandard stop codons beginning with adenine in vertebrate mitochondria. *RNA* 2010;16:1146–1155.
44. Gagnon MG, Seetharaman SV, Bulkley D, Steitz TA. Structural basis for the rescue of stalled ribosomes: structure of YaeJ bound to the ribosome. *Science* 2012;335:1370–1372.
45. Wredenberg A, Wibom R, Wilhelmsson H, Graff C, Wiener HH, Burden SJ, Oldfors A, Westerblad H, Larsson NG. Increased mitochondrial mass in mitochondrial myopathy mice. *Proc Natl Acad Sci USA* 2002;99:15066–15071.
46. Auré K, Fayet G, Leroy JP, Lacène E, Romero NB, Lombès A. Apoptosis in mitochondrial myopathies is linked to mitochondrial proliferation. *Brain* 2006;129:1249–1259.
47. Gray MW, Burger G, Lang BF. Mitochondrial evolution. *Science* 1999;283:1476–1481.